Citation: Rehrl C., and G. Kirchengast: Mesospheric Temperature and Ozone Sounding by the SMAS Solar Occultation Sensor, in: Occultations for Probing Atmosphere and Climate (G. Kirchengast, U. Foelsche, A.K. Steiner, eds.), Springer, Berlin-Heidelberg, 333-342, 2004.

Mesospheric Temperature and Ozone Sounding by the SMAS Solar Occultation Sensor

C. Rehrl and G. Kirchengast

Institute for Geophysics, Astrophysics, and Meteorology (IGAM), University of Graz, Austria
christoph.rehrl@uni-graz.at

Abstract. We discuss a realistic forward modelling and retrieval algorithm for temperature and ozone sounding developed to process data received by the planned Sun Monitor and Atmospheric Sounder (SMAS) instrument. The SMAS sensor concept employs the solar occultation technique and is primarily aiming at mesospheric profiles. The SMAS sensor provides self-calibrating transmission data, which allows the accurate derivation of profiles of molecular oxygen, molecular nitrogen, atomic oxygen, and ozone and temperature. We concentrated on data between 180 nm and 250 nm to analyse transmission data for ozone and temperature profiling. In order to enable a good and fast retrieval algorithm performance, a detailed view of the absorption behaviour of the solar irradiance in the considered wavelength region is necessary and will be presented in this work. In particular, some emphasis is placed on evaluating different fast forward modelling approximations for the SMAS channels in the Schumann-Runge bands (180–205 nm). Exemplary retrieval results for ozone are shown as well.

1 Introduction

Absorptive occultation data bear great capability of providing profiles of atmospheric key quantities like temperature and trace gases such as ozone (e.g., Smith and Hunten 1990). Absorption of solar radiation at wavelengths from 180 to 250 nm has a substantial impact in the photochemistry of the middle atmosphere. The SMAS sensor concept uses solar occultation, an active limb sounding technique with the sun as the source of radiation and satellite photo-detectors as sensors, and with the Earth's atmosphere between acting as the absorption "cell". The SMAS sensor is mounted aboard a low-Earth-orbiting satellite, and it measures the intensity of the solar light while the sunrays are occulted by the atmospheric limb of the Earth, either during sunrise (rising occultation event) or sunset (setting occultation event). The transmission profile (normalised intensity) thus obtained contains information about the combined limb path column density of all absorbing species.

The SMAS ultraviolet (UV) occultation sensor uses the middle and extreme UV wavelength region. This implies that SMAS aims at exploiting the interaction of the middle and upper atmosphere with the incoming solar radiation; in this study the focus is on the mesosphere, where attenuation due to absorption by molecular oxygen and ozone is exploited.

The intensity of the solar radiation passing the Earth's atmosphere is given by the combined attenuation of all absorbing species along the ray path and can be basically determined using the Beer-Bouguer-Lambert's law, at each frequency ν, as

$$T_\nu = \frac{I_\nu(z)}{I_\nu(0)} = \exp\left(- \int_{sun}^{leo} \sum_i n_i(s)\sigma_{i\nu}(s)ds \right). \quad (1)$$

The transmission T_ν at any given wavelength is a ratio of the solar radiation intensity measured in the atmosphere, $I_\nu(z)$ (z, ray tangent height), relative to the solar intensity above the atmosphere, $I_\nu(0)$ (in practice measured at a height of ~120 km in case of SMAS). While the satellite is moving in its orbit, the occultation rays dive deeper and deeper into the atmosphere (given a setting event as example) and the signal intensity gradually decreases. The integral is carried out along the ray path *s*, which is slightly refracted for altitudes up to ~75 km, above which refraction and thus bending of the rays is negligible. The number densities n_i and the cross sections $\sigma_{i\nu}$ are associated with the primary mesospheric absorbers molecular oxygen (O_2) and ozone, which largely determine the transmission seen by the SMAS sensor.

Furthermore, a (small) term for Rayleigh scattering is included but the term for aerosol extinction can be neglected. In this basic work the small nitric oxide photodissociation structures near 191 nm and 183 nm (see, e.g., Minschwaner and Starke 2000), constituting the primary mechanism for NO_x removal in the middle atmosphere, are disregarded but might be accounted for in a future refinement.

2 Channel Selection

Based on a sensor analysis for the SMAS sensor concept, the radiometric channels of the instrument are selected as summarised in the Table 1 below. The examination of the radiative interaction properties due to the Earth's atmosphere suggests a natural range in the wavelength region less than 250 nm. For the mesospheric heights of interest from 50 to 100 km, the relevant spectral features for O_2 are the Schumann-Runge (SR) bands and the Herzberg continuum, for ozone it is the lower edge of the Hartley band.

Figure 1 shows the optical thickness of the absorbing species in the UV region between 175 and 250 nm at an tangent height of 60 km. The O_2 density used here was calculated from the CIRA-86 model (March, 40 deg N) and the ozone density was based on AFGL-TR-86 data (standard mid-latitude profile).

As Table 1 indicates, the core channels for temperature and ozone retrieval are the SMAS channels 7 to 14. The baseline width of these channels is 5 nm and the spectral locations of and distances between the channels are defined such that, in terms of transmission sensitivity, complete coverage of the mesospheric height domain is ensured (Rieder and Kirchengast 2001; see also Sect. 3).

Channel Number	Channel Wavelength [nm]	Solar origin of radiation	Main solar emission	Atmospheric species intervening in occultation
1 (EUV)	**1 – 10**	**Corona**		**N_2, O_2, O**
2 (EUV)	**17 - 25**	**Corona**	**Fe X - Fe XII**	**N_2, O**
3 (EUV)	**29 – 35**	**Transition region**	**He II (30.4 nm)**	**N_2, O**
4 (EUV)	**50 –65**	**Chromosphere**	**He I (58.4 nm)**	**N_2, O**
5 (EUV)	**70 – 90**	**Transition region**	**O II – O IV**	**N_2, O**
6 (EUV)	**110 – 130**	**Chromosphere**	**H I (121.6 nm)**	**O_2**
7 (MUV)	184±2.5	Photosphere	Continuum	O_2
8 (MUV)	190±2.5	Photosphere	Continuum	O_2
9 (MUV)	195±2.5	Photosphere	Continuum	O_2, O_3
10 (MUV)	200±2.5	Photosphere	Continuum	O_2, O_3
11 (MUV)	205±2.5	Photosphere	Continuum	O_3, O_2
12 (MUV)	210±2.5	Photosphere	Continuum	O_3, O_2
13 (MUV)	224±2.5	Photosphere	Continuum	O_3
14 (MUV)	246±2.5	Photosphere	Continuum	O_3
15 (VIS)	**300-700**	**Photosphere**	**Continuum**	**Air**

Table 1. Channel selection for the SMAS sensor concept. The MUV channels of interest in this study are highlighted (SMAS channels 7 to 14).

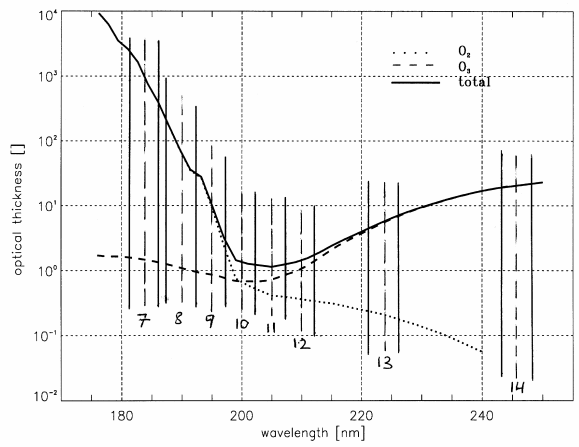

Fig. 1. Optical thickness of molecular oxygen, ozone, and of both together at 60 km height.

3 SMAS Transmission

The transmission for any given individual measurement can be modelled as

$$T(t_i) = \int_{\Delta t}\int_{\Delta \upsilon}\int_{\Delta \lambda} T_{atm}(\lambda, \upsilon, t) W(\lambda - \lambda_0) W_\upsilon W_t \, d\lambda \, d\upsilon \, dt \,, \tag{2}$$

where the transmission profile is sampled as a function of time t_i. By geometry, each sampling time corresponds to a specific tangent height. The basic sampling rate in case of the SMAS sensor is 10 Hz and corresponds to a vertical sampling of about 200 m. The integral is carried out over a wavelength band $\Delta\lambda$, properly covering the spectral width of each channel, the vertical field-of-view $\Delta\upsilon$, and the measurement integration time per sample, Δt. The SMAS field-of-view is pointing to sun centre and designed 1/30 deg wide, corresponding to ~2km vertical resolution. This limited field-of-view covering only an equatorial fraction of the solar disk (< 20 deg band) is useful, since the full solar disk would otherwise illuminate at any given time a height range of 25-30 km extend, severely complicating the retrieval of atmospheric profiles (Lumpe et al 1991). The channel shape function $W(\lambda\text{-}\lambda_0)$ is modelled as (normalized) Gaussian function with a half-width of 2.5 nm. Furthermore, two simple boxcar functions are used, $W=1/\Delta\upsilon$ ($\Delta\upsilon = 1/30$ deg) and $W=1/\Delta t$ (Δt = 0.1 sec), for properly limiting the field-of-view and time integration domains.

For given geometry and time t_i, the atmospheric transmission field $T_{atm}(\lambda,\upsilon,t)$ can be sampled as function of wavelength, field-of-view, and time, and then integrated according to Eq. 2 to obtain the desired channel transmission $T(t_i)$. For the smooth atmospheric profiles adopted in this study, the two boxcar integrations could be ignored and T_{atm} was just a forward model calculation for different wavelengths along a single ray arriving from sun centre at time t_i.

The SR band region is of central importance to the absorption of solar radiation by O_2 and in determining ozone concentrations. The SR bands control the limb absorption in the mesosphere from about 60 km to 100 km. The absorption system is characterised by a banded structure from 174 nm to 204 nm. The SR absorption cross section varies by about four orders of magnitude between 174 nm and 204 nm. The band system shows a regular appearance at longer wavelengths, because there exists a regularity of the spacing of vibrational and rotational energy levels. At shorter wavelengths, the number of lines from overlapping bands becomes so big that the spectrum has a quasi-random appearance. Furthermore, the SR absorption cross sections exhibit a temperature dependence, which is strongest between 192 nm and 204 nm. Figure 2, left panel, depicts the O_2 absorption cross sections in the SR region for a temperature of 240 K. The SR cross section data were taken from Minschwaner et al. (1992), computed from polynomial coefficients, including the Herzberg continuum cross section in the region between 185 nm and 204 nm. Regarding wavelengths > 204 nm, the Herzberg continuum data were taken from Nicolet et al (1989) and the ozone cross section data from Molina and Molina (1986), respectively.

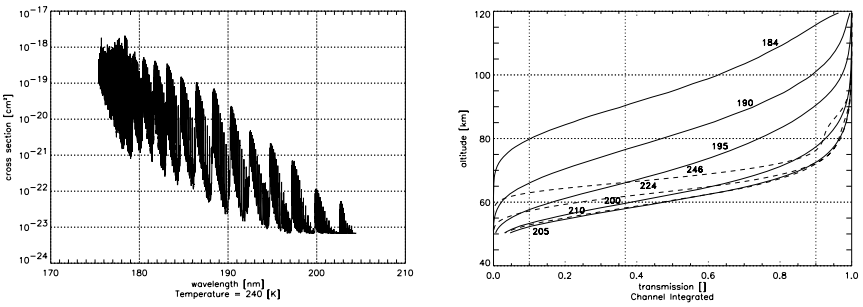

Fig. 2. Spectral distribution of the absorption cross section of molecular oxygen in the Schumann-Runge bands (left panel) and modelled SMAS transmission profiles (right panel). In the right panel, the solid lines show the transmission profiles in the Schumann-Runge bands and the dashed lines show the transmission profiles in the Herzberg continuum and overlapping Hartley band. The annotated numbers denote the centre wavelengths of the channels. The vertical dashed lines near the left and right boundary delimit the region, within which measurements are foreseen to be exploited.

Figure 2, right panel, shows exemplary SMAS transmission data modelled on the basis of a realistic occultation event. The geometry data of the event were computed by an enhanced EGOPS (End-to-end Generic Occultation Performance Simulator) (Kirchengast 1998; Kirchengast et al 2002), an occultation software tool currently under development from version 4 (Kirchengast et al 2002) to Version 5. Furthermore, spherically symmetric atmospheric profiles were adopted and a scanning of the atmosphere over altitudes from 120 km to 50 km was used.

For an exact calculation of the transmission profiles in the highly oscillatory SR bands, a resolution of 3000 sampling points (0.002 nm sampling) for each channel is necessary. Using these 3000 samples of T_{atm}, Figure 2, right panel, shows the wavelength-integrated channel transmission profiles. For the channels > 205 nm, the absorption cross sections are smooth functions – O_2 Herzberg continuum and ozone Hartley band – and 0.2 nm sampling is sufficient. The Herzberg continuum comprises the wavelength region between 185 and 242nm, the Hartley band those from ~190 to 310 nm, reaching a maximum near 250 nm. Because of the large number density of O_2 compared to ozone, the Herzberg continuum is important beyond 205 nm even though the cross section is small relative to the ozone cross section in the Hartley band (indicated also by the optical thicknesses illustrated in Fig. 1). The Hartley band absorption is unimportant below ~190 nm. The cross sections in the Herzberg continuum and Hartley band show a very slight temperature dependence, which can be neglected in the SMAS forward modelling.

As a result of the dense sampling needed in the SR bands, the rigorous forward model algorithm is fairly slow, and if used as part of an inversion algorithm a faster algorithm is highly desirable. In order to obtain such a faster algorithm, we evaluated the following two approximations: the piecewise integration approximation (PIA) and the optimal random selection approximation (ORSA).

3.1 Piecewise Integration Approximation (PIA)

In the PIA, SR cross sections integrated over a prescribed number of partial channels of width $\Delta\lambda$, spread over the full spectral width of a SMAS SR channel, are used to compute the channel transmissions. The needed values of the Gaussian channel shape function are properly averaged as well.

More explicitly, the PIA approximates channel transmissions $T_{ch}(s)$ as follows,

$$T_{ch}(s) = \sum_{i=\Delta\lambda_i}^{\Delta\lambda_I} T_{ch,i}(s) = \sum_{i=\Delta\lambda_i}^{\Delta\lambda_I} \exp(-\int_s \overline{\sigma}(\Delta\lambda_i, T(s)) n(s) ds) \overline{W}(\Delta\lambda_i) \,, \tag{3}$$

with the associated averaged temperature-dependent SR absorption cross section $\overline{\sigma}(\Delta\lambda_i, T(s))$,

$$\overline{\sigma}(\Delta\lambda, T(s)) = \frac{1}{\Delta\lambda} \int_{\Delta\lambda} \sigma(\lambda, T(s))\, d\lambda \,, \tag{4}$$

and averaged Gaussian weighting function $\overline{W}(\Delta\lambda_i)$, given by

$$\overline{W}(\Delta\lambda) = \frac{1}{\Delta\lambda} \int_{\Delta\lambda} W(\lambda - \lambda_0) d\lambda \,, \tag{5}$$

$$\sum_{i=\Delta\lambda_i}^{\Delta\lambda_I} \overline{W}(\Delta\lambda_i) = 1 \cdot \tag{6}$$

Both, the averaged SR absorption cross sections and the Gaussian weighting function are integrated over a finite equidistant wavelength region $\Delta\lambda$ for each partial channel. In turn, according to Eq. 3, all partial channel transmissions are integrated to yield the full channel transmission. Figure 3, left panel (to be compared with Figure 2, left panel) illustrates integrated SR cross sections as used in the PIA (Eq. 4), for 30 partial channels (0.2 nm sampling). Resulting transmission profiles for the five SMAS SR channels are shown in Fig. 3, right panel, for different numbers of partial channels.

The primary band structure of the SR bands persists to a certain degree under the PIA integration as Fig. 3, left panel, illustrates. Figure 3, right panel, shows, though, that a sufficient number of partial channels is needed to accurately model the transmission. While 30 partial channels are clearly not yet such a sufficient number, 300 partial channels appear to be an adequate number already, furnishing an accuracy of the approximated transmission of better than 1%. Compared to original 3000 bins per channel this is a reduction by a factor of 10 of the computational cost for sampling T_{atm}. The use of the PIA in a forward model embedded in retrieval algorithms is simple and straightforward.

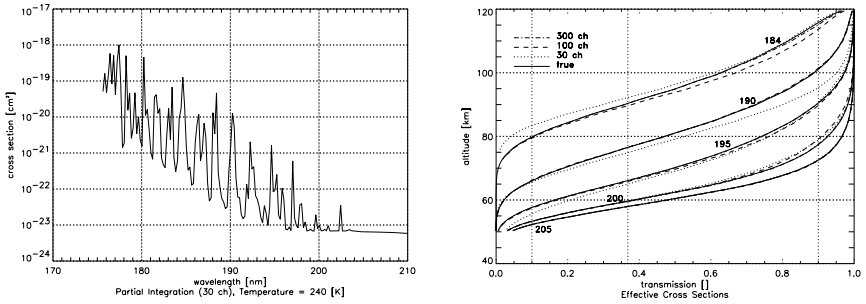

Fig. 3. Left panel – partially integrated Schumann-Runge absorption cross sections at 240 K, for 30 partial channels. Right panel – transmission profile in the Schumann-Runge bands for full integration (true), 30 partial channels (dotted), 100 partial channels (dashed), and 300 partial channels (dashed-dotted).

3.2 Optimal Random Selection Approximation (ORSA)

The idea of the ORSA is to reduce the number of sampling bins by Monte-Carlo drawing of a prescribed number of bins out of the original sample of 3000 bins. Using this Monte-Carlo drawing, for which 10000 trials were found to be an adequate number of trials, we targeted to reduce the 3000 bins per SR channel to an optimal subset of 100 bins, i.e., a further factor of 3 less than what was found to be needed in case of the PIA discussed above. Optimality is defined in that we keep that 100-bin subset from the 10000 randomly drawn subsets, which produces for a given atmospheric state (temperature profile) the most accurate approximated channel transmission profile compared to the exact 3000-bin per channel computation. Performing this type of ORSA for a sufficient diversity of atmospheric temperature profiles provides a number of look-up tables, which can be used in a nearest-neighbour sense for a fast algorithm based on only 100 bins per SR channel.

Figure 4 illustrates the ORSA performance for a few exemplary atmospheric conditions, based on CIRA86 profiles; the month and latitude of the profiles used is noted at each sub-panel. The left set of four sub-panels shows results for January/Equator as “true” reference, the right set for July/80 deg North. The upper-left sub-panel in both cases shows the baseline accuracy, where the ORSA results for the “true” conditions are shown. By using conditions a month and some latitudinal distance apart from the “true conditions”, the other sub-panels mimic the more realistic situation, where the ORSA selection is based on a priori knowledge of conditions only. A set of 18 conditions over different months and latitudes seems to be sufficient for ensuring an accuracy in approximated transmissions of better than 1% for the SMAS SR channels based on 100 bins. Whether the factor of 3 advantage, in terms of reduction of bins, of the ORSA over the PIA justifies its preferred use despite of its more complicated handling (diversity of look-up tables, etc.) will be decided in the context of retrieval algorithm evaluations.

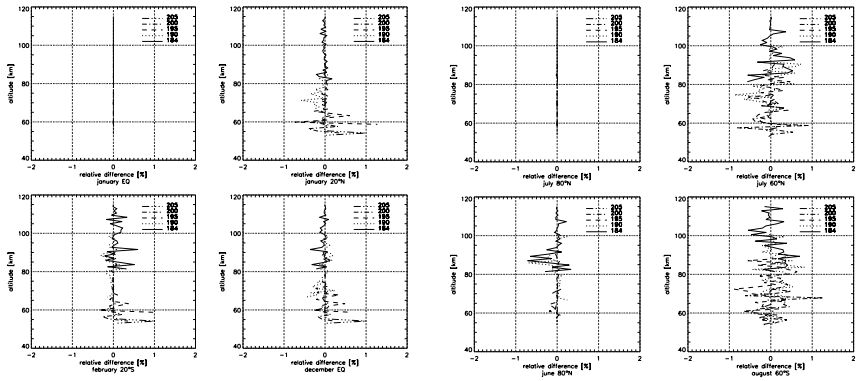

Fig. 4. Illustration of ORSA performance for a few exemplary atmospheric conditions (January/Equator, July/80 deg North). Each sub-panel shows the accuracy of the ORSA relative to the exact forward model results, which have been taken as "true" reference.

4 Results – Ozone Retrieval

We present first retrieval results, derived from the SMAS Hartley band channels 12 to 14, where the primary absorber is ozone (see Sect. 2). These three channels involve smoothly varying cross sections. The retrieval algorithm preparations for the SR channels and the joint temperature and ozone retrieval based on all eight SMAS MUV channels are currently on-going.

A sequential inversion process was applied, starting with a spectral inversion of transmissions to O_2 and ozone slant columns, followed by a vertical inversion via an Abel transform to obtain an ozone number density profile from the ozone columnar content. Monitoring of the mesosphere by the SMAS solar occultation sensor starts with the measurement of signal intensity profiles normalized to transmission profiles, one for each channel.

The spectral inversion converts the transmission data only for the three Hartley channels case into columnar contents describing the horizontally-integrated vertical distribution of the two absorbers O_2 and ozone, where the former is a by-product only in this Hartley channels case.

Proceeding with the vertical inversion, the Abel integral was discretised into matrix form, assuming that the derivatives of the ozone number density vary linearly inside each layer. The resulting ozone density profile for an exemplary case is illustrated in Fig. 5, left panel, and differences between retrieved and "true" profiles are shown in Fig. 5, right panel. Different typical radiometric noise levels were assumed, based on the expected performance characteristics of the SMAS photo-detectors.

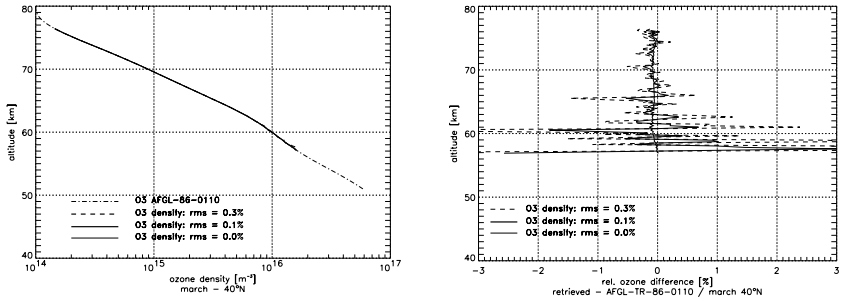

Fig. 5. SMAS-retrieved ozone profile (left panel) and relative difference between retrieved profiles and "true" profile for different sensor noise levels (right panel). A standard (AFGL) mid-latitude ozone profile was used as "true" profile.

The Abel transform from columnar content to number density data is sensitive to noise in input data and thus moderately amplifies noise in the transmission data.

As summarized by Rieder and Kirchengast (2001), the expected noise on unattenuated solar intensity measurements at 180 nm at a sampling rate of 10 Hz is 0.03% for diamond photo-diodes and 0.1% for silicon photo-diodes. The noise corresponds to Gaussian white noise. The transmission noise levels assumed for Fig. 5 are noted as rms errors in the panels: 0.1% is representative for silicon diodes, 0.3% leaves some margin for further error sources (e.g., residual cross section uncertainties). The small baseline retrieval error for 0% noise (light solid line) indicates residual numerical errors, in the present preliminary algorithm mostly due to the departure of the discretised solution of the Abel transform from the analytical solution. A relative ozone retrieval error of less than 1% in most of the height domain of interest is found for the 0.1% measurement error case. This is encouraging for the joint temperature and ozone retrieval algorithm currently prepared.

In summary, the SMAS sensor concept bears great capability to monitor mesospheric temperature and ozone with high vertical resolution and accuracy.

Acknowledgements. The authors gratefully acknowledge valuable discussions with and support by C. Retscher, U. Foelsche, M. Schwaerz, and J. Ramsauer (IGAM, Univ. of Graz, Austria). C.R. received financial support for the work from ENVISAT Project AO-620/Part-I funded by the Austrian Ministry for Traffic, Innovation, and Technology and carried out under contract with the Austrian Space Agency.

References

Kirchengast G (1998) End-to-end GNSS Occultation Performance Simulator overview and exemplary applications. Wissenschaftl Ber 2/1998, IGAM, Univ of Graz, Austria, 138 pp

Kirchengast G, Fritzer J, Ramsauer J (2002) End-to-end GNSS Occultation Performance Simulator version 4 (EGOPS4) software user manual (overview and reference manual). Tech Rep ESA/ESTEC-3/2002, IGAM, Univ of Graz, Austria, 472 pp

Lumpe JD, Chang CS, Strickland DJ (1991) Atmospheric constituent density profiles from full disk solar occultation experiments. J Quant Spectrosc Rad Transfer 46: 483-506

Minschwaner K, Anderson GP, Hall LA, Yoshino K (1992) Polynomial Coefficients for Calculations. J Geophys Res 97: 10103-10108

Minschwaner K, Starke V (2000) Photodissociation of nitric oxide in the middle and upper atmosphere. Phys Chem Earth manuscript no ST9.2-022, Dept of Physics, New Mexico Inst of Mining and Technology, Socorro, New Mexico

Molina LT, Molina MJ (1986) Absolute absorption cross sections of ozone in the 185- to 350-nm wavelength range. J Geophys Res 91: 14501-14508

Nicolet M, Cielik S, Kennes R (1980) Atmospheric absorption in the O_2 S-R band spectral range and photodissociation rates in the stratosphere and mesosphere. Planet Space Sci 28: 85-103

Rehrl C (2000) Mesospheric temperature and ozone sounding based on solar occultation data. M Sc thesis, 124 pp, IGAM, Univ of Graz, Austria

Rieder MJ, Kirchengast G (2001) Error analysis for mesospheric temperature profiling by absorptive occultation sensors. Ann Geophys 19: 71-81

Smith GR, Hunten DM (1990) Study of planetary atmospheres by absorptive occultations. Rev of Geophys 28: 117-143